Three-dimensional numerical models with varied material properties and erosion rates: Implications for the mechanics and kinematics of compressive wedges

Phaedra Upton,[1,2] Karl Mueller,[3] and Yue-Gau Chen[4]

Received 19 March 2008; revised 29 January 2009; accepted 13 February 2009; published 21 April 2009.

[1] We develop three-dimensional mechanical models of a compressive wedge and investigate how the form and kinematics of the outboard wedge are affected by variation in initial topography, material properties, and erosion rate. Inclusion into the wedge of weaker, less dense material affects the form of the wedge, producing a region of steeper average slopes and higher topography while depriving the region further inboard of material. Enhanced erosion has a similar effect. The wedge attempts to replace the eroded material by focusing deformation. The result is a stepped region of lower topography within the outboard of the orogen. We observe that uplift velocities at three points in the orogen vary cyclically from near zero to ~3 times the average uplift rate over cycles lasting on the order of 15–200,000 model years. Our models, along with analog models and some well-dated examples from active orogens, suggest that transient accommodation of strain may be common. The cycles observed responded rapidly to changes in the amount of erosion imposed. Our models suggest that orogens may be driven by strong coupling between erosion and strain on temporal scales of 10^4–10^5 years and spatial scales comparable to the scale of the erosional perturbation. We compare our models to the Puli Embayment of west central Taiwan, a region of anomalous low topography and suggest that it presence may reflect the presence of weaker and more erodible sediments than those present along strike in the orogen.

Citation: Upton, P., K. Mueller, and Y.-G. Chen (2009), Three-dimensional numerical models with varied material properties and erosion rates: Implications for the mechanics and kinematics of compressive wedges, *J. Geophys. Res.*, *114*, B04408, doi:10.1029/2008JB005708.

1. Introduction

[2] The topography of a critically tapered compressive orogenic belt reflects the coupled interaction between rock uplift and erosion [*Koons*, 1990; *Willett et al.*, 1993]. In an active orogen, variation in topography along strike reflects change in one or more of the parameters which control these two processes. Parameters can include the strength of the underlying décollement, the rheology of the deforming wedge, and the tectonic and/or surficial boundary conditions. It is often difficult to adequately characterize boundary conditions from available observations in order to isolate which of the controlling parameters drives transient stress and/or strain states in an orogen, particularly if two or more parameters are involved.

[3] Dynamic coupling between climate-driven erosion and tectonics in an active orogen can strongly influence landscape evolution within the resulting mountain belt [e.g., *Koons*, 1990; *Willett et al.*, 1993; *Koons et al.*, 2002, 2003; *Thiede et al.*, 2004; *Grujic et al.*, 2006]. This has been demonstrated using numerical [*Avouac and Burov*, 1996; *Willett*, 1999; *Koons et al.*, 2002, 2003] and analog [*Hoth et al.*, 2006] modeling, as well as through a number of field studies, particularly those utilizing fission track and other geochronologic methods [*Zeitler et al.*, 2001; *Thiede et al.*, 2004, 2005; *Grujic et al.*, 2006; *Berger and Spotila*, 2008; *Berger et al.*, 2008]. Despite recognition of the importance of coupling between tectonic and surfical processes, surprisingly little direct data exists for assessing exactly how an orogen responds to transient changes in boundary conditions, such as a change in the erosion rate. Nor have the scales at which an orogen might respond to transient changes in boundary conditions at the surface, such as evolving river networks, been well constrained.

[4] Numerical and analog models are particularly valuable as we attempt to unravel the complexities of dynamically coupled systems in geology. Each has their own advantages and disadvantages. Analogue models are inherently three-dimensional and can usually be run to large strains, they are visual and, with the use of CT scanning, can

[1]Department of Earth Sciences, University of Maine, Orono, Maine, USA.
[2]Now at GNS Science, Dunedin, New Zealand.
[3]Department of Geological Sciences, University of Colorado, Boulder, Colorado, USA.
[4]Department of Geosciences, Taiwan National University, Taipei, Taiwan.

0148-0227/09/2008JB005708$09.00

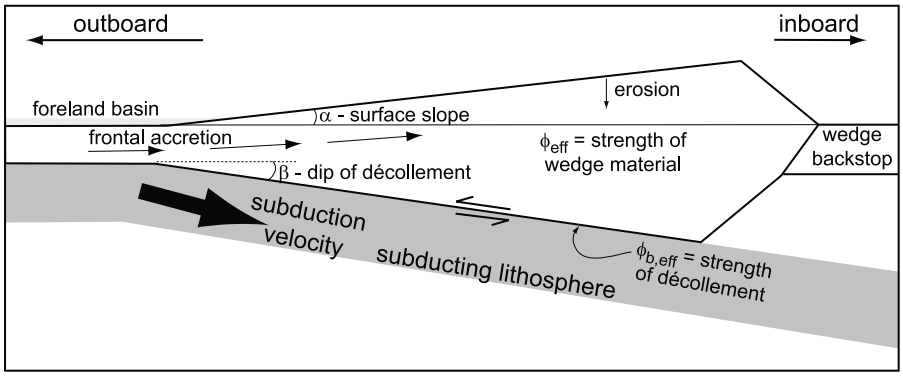

Figure 1. Geometric parameters of a subaerial critical wedge in two dimensions. The wedge grows by frontal accretion as undeformed material from the foreland basin is incorporated into the wedge [*Davis et al.*, 1983].

yield approximations of the 3-D strain, strain rate and other parameters [e.g., *Marques and Cobbold*, 2002; *Soto et al.*, 2006a, 2006b; *Hoth et al.*, 2006, 2007]. Numerical solutions allow the models to be interrogated at any point in time or space to yield velocities, stresses, strain, strain components, etc. However, because of the large computational demands required by orogen-scale numerical solutions, models are typically run in a two-dimensional across-strike orientation. In this study, we use three-dimensional numerical models to test how various changes in controlling parameters, in particular wedge rheology and erosion rates, can affect strain in a model fold and thrust belt.

[5] Having analyzed the results of our numerical analysis, we then compare the model behavior to the Late Quaternary development of west central Taiwan. This portion of the Taiwanese thrust belt is marked by a 50-km-wide topographic low, termed the Puli Embayment [*Upton et al.*, 2003b]. We suggest that dynamic coupling between the material incorporated into the thrust belt and the imposed pattern of erosion may contribute to the development of the area of lower topography in the Puli region.

2. Controls on Wedge Form

[6] Accretionary wedges and fold and thrust belts around the globe can be characterized to a first order by critical wedge theory [*Chapple*, 1978; *Stockmal*, 1983; *Davis et al.*, 1983; *Dahlen*, 1984; *Dahlen et al.*, 1984]. The geometric description of an orogenic wedge is based on the angle of inclination of the basal décollement β and that of the surface α (both relative to horizontal) (Figure 1). Wedges develop their characteristic form because deformation can take place either along the décollement or within the wedge. If the internal strength of the wedge is greater than that of the basal décollement, then the wedge will be translated as an undeformed mass. If the internal strength of the wedge is weaker than that of the basal décollement, then the wedge deforms internally and the surface topographic slope will increase. If the wedge is composed of a pressure-dependent rheology, its strength will increase as the thickness of the wedge increases, eventually reaching a critical taper between the surface and base where the strength of the wedge is equal to the strength of the basal décollement [e.g., *Davis et al.*, 1983; *Dahlen et al.*, 1984]. In this state, the wedge can move along the décollement and widen, while maintaining its shape during progressive deformation.

[7] The shape of the wedge can be predicted if we know the values of certain parameters including the basal friction, the strength of the wedge, internal pore pressure and fluxes of material moving into and out of the wedge [*Chapple*, 1978; *Stockmal*, 1983; *Davis et al.*, 1983; *Dahlen*, 1984]. A weak décollement will result in a low lying, broad wedge, whereas as a stronger décollement will form a steeper, narrower wedge [*Chapple*, 1978; *Stockmal*, 1983; *Davis et al.*, 1983; *Dahlen*, 1984]. Many studies have shown that erosional processes also exert an important control on the form of the wedge [e.g., *Dahlen and Suppe*, 1988; *Dahlen and Barr*, 1989; *Koons*, 1990, 1995; *Beaumont et al.*, 1992; *Willett and Beaumont*, 1994; *Avouac and Burov*, 1996; *Willett*, 1999]. Wedges formed at the scale of orogens appear to be partially controlled by the ratio of accretionary flux to erosional efficiency [*Hilley and Strecker*, 2004; *Whipple and Meade*, 2004]. As this ratio is increased, wedge width and surface slope increase [*Hilley and Strecker*, 2004]. Concentration of erosion on windward slopes can control orogen shape, surface rock uplift rates and strain partitioning within a doubly vergent orogen [e.g., *Koons*, 1990; *Beaumont et al.*, 1992, 1996; *Willett*, 1999; *Willett and Beaumont*, 1994; *Koons et al.*, 2002, 2003; *Upton and Koons*, 2007]. For example, an orographic rainfall system developed as the Southern Alps of New Zealand have been uplifted produces high rates of erosion along the western edge of the mountain range. The high erosion rates maintain material removal and deformation along the Alpine Fault [*Koons*, 1990; *Beaumont et al.*, 1992]. Many recent studies also suggest that focused erosion along the Himalayan front also may have an effect on the nature and locus of the deformation [e.g., *Thiede et al.*, 2004, 2005; *Wobus et al.*, 2003, 2005], although other authors argue against erosion playing such as controlling role [e.g., *Burbank et al.*, 2003].

[8] The majority of previous studies which investigate the controls on wedge form have considered two-dimensional analytical models of wedges with uniform properties and/or uniform erosion conditions [e.g., *Davis et al.*, 1983; *Dahlen et al.*, 1984; *Dahlen*, 1984; *Hilley and Strecker*, 2004; *Whipple and Meade*, 2004]. In this study, we are interested in variations in both wedge properties and erosional flux,

along strike and across the wedge, and we use a numerical rather than an analytical approach.

3. Modeling Methods

3.1. Mechanical Models

[9] We model a generic fold and thrust belt using a simplified geometry consisting of an elastic slab, representing the basement of a subducting plate, beneath an elasto-plastic Mohr-Coulomb wedge, representing passive margin sediments (Figure 2a). The two blocks are separated by an interface along which frictional slip can occur but no material exchange takes place across it. The solution domain is a three-dimensional numerical region extending 220 km normal to the plate boundary (= x) by 250 km parallel to the plate boundary (= y) by 18 km vertically (= z). The eastern edge of the model consists of an elastic block simulating a rigid indentor, such as a colliding volcanic arc, that does not deform internally to a significant extent. Our models are aimed primarily at unraveling the style of crustal deformation in the outboard (or prowedge) of such a collision, away from the actual plate boundary [*Koons*, 1990; *Willett et al.*, 1993]. Note that these models do not consider the whole period of orogen development, having a starting point when the main divide region is already well developed (Figure 2b). Our initial topography of 2000 m elevation at the main divide was chosen to ensure that deformation would occur above the shallower portions of the décollement. This was a necessity of the modeling method, in which we are limited as to the maximum amount of strain we can run to.

3.2. Material Properties

[10] Sediments making up the upper plate are modeled using a Mohr-Coulomb rheology, a pressure-dependent material description in which strength increases with increasing depth (Table 1). We use an effective friction angle (ϕ_{eff}) to describe the strength of the material that includes the effect of internal pore pressure. Movement along the basal décollement is also defined by an effective friction angle ($\phi_{\text{b,eff}}$). Values for our base model are ρ = 2600 kg/m^3, $\phi_{\text{eff}} = 16°$ and $\phi_{\text{b,eff}} = 5°$ derived from the Taiwanese accretionary prism [*Carena et al.*, 2002]. We run a series of sensitivity models, varying these values from $\phi_{\text{eff}} = 13°$ to 20° and $\phi_{\text{b,eff}} = 3°$ to 10°.

[11] We incorporate a volume of lower-density material into the wedge to mimic a sedimentary basin comprising slightly weaker sediments, such as might have been incorporated into a wedge as it propagated into a foreland. This region consists of material with ρ = 2400 kg/m^3 (relative to 2600 kg/m^3 in surrounding regions) and $\phi_{\text{eff}} = 14°$ (Figure 2).

3.3. Velocity Boundary Conditions

[12] Velocity boundary conditions are imposed upon the elastic block that represents the underlying subducting slab (Figure 2a). This block is pushed with a generic velocity of 20 mm/a orthogonal to the boundary between the wedge and the indentor. Twenty millimeters per year was chosen as a moderate convergence velocity for accretionary prisms. The wedge material separated from this downgoing plate by the décollement, a planar feature represented in the model by an interface along which relative motion can take place. Within the wedge, two regions of deformation develop: (1) relatively focused deformation close to the indentor and (2) a region of distributed deformation within the wedge, at a distance from the indentor. It is the latter deformation that we focus on in this study. The lateral boundaries (y = 0) have a fixed velocity condition and are located well away from the studied region in the models.

[13] Our models resemble a numerical sandbox and are similar to the analog models run by *Hoth et al.* [2006] and discrete element models of *Naylor and Sinclair* [2007] in that the lower boundary is fixed in space. The model does not attempt to simulate isostatic compensation for the topography and the base of the model cannot adjust itself even though topography increases with ongoing strain. Thus, while the wedge widens with time, topography continues to build slowly, approaching a steady state value more slowly than is seen in nature.

3.4. Erosional Boundary Conditions

[14] Erosion rates in active fold and thrust belts vary from <1 mm/a (e.g., eastern Southern Alps, New Zealand [*Hicks et al.*, 1996]; Antiplano, Bolivia [*Ege et al.*, 2007; *Safran et al.*, 2006]; and European Alps [*Bernet et al.*, 2001]) to >5 mm/a (e.g., Alpine Fault, New Zealand [*Hovius et al.*, 1997], and eastern Taiwan [*Galewsky et al.*, 2006]; *Fuller et al.*, 2006; *Dadson et al.*, 2003]) and in extreme cases >10 mm/a (St Elias Mountains, Alaska [*Spotila et al.*, 2004; *Berger and Spotila*, 2008]). Erosion is often asymmetric and for our models we use a generic scheme that seeks to mimic the asymmetric exhumation of many two-sided orogens, such as the Southern Alps of New Zealand [*Hicks et al.*, 1996; *Hovius et al.*, 1997], central Taiwan [*Liu et al.*, 2001; *Galewsky et al.*, 2006; *Fuller et al.*, 2006], the St Elias Mountains [*Sheaf et al.*, 2003; *Spotila et al.*, 2004], and the Andes [*Masek et al.*, 1994; *Ege et al.*, 2007; *Safran et al.*, 2006].

[15] Erosion is imposed onto the top surface of the model as an imposed boundary condition. Material is removed from the model by lowering of grid points. We chose rates ranging between 1 and 3 mm/a for our models (Figure 2b). An erosion rate of 1 mm/a is imposed upon the western part of the orogen and 1.3 mm/a is imposed on the eastern part of the orogen. Within the region of interest, erosion is varied both spatially and temporally.

[16] These models do not attempt to relate the erosion to any particular erosion law. We assume a constant erosion rate over the area we are eroding for the time of the model. We are simply interested in the effect of material removal on the dynamics of the fold and thrust belt rather than the interaction between varied rates of erosion and topography. Such interactions are interesting and important for finer scale studies of the orogen, however, the complexities of numerically coupling these processes are beyond the scope of this study and are the subject of current model development.

3.5. Solution Method

[17] Models were developed using the numerical code FLAC^{3D} [*Itasca*, 2006], which we have modified to accommodate local erosion as described above. Results from FLAC^{3D} are based upon fully three-dimensional solutions

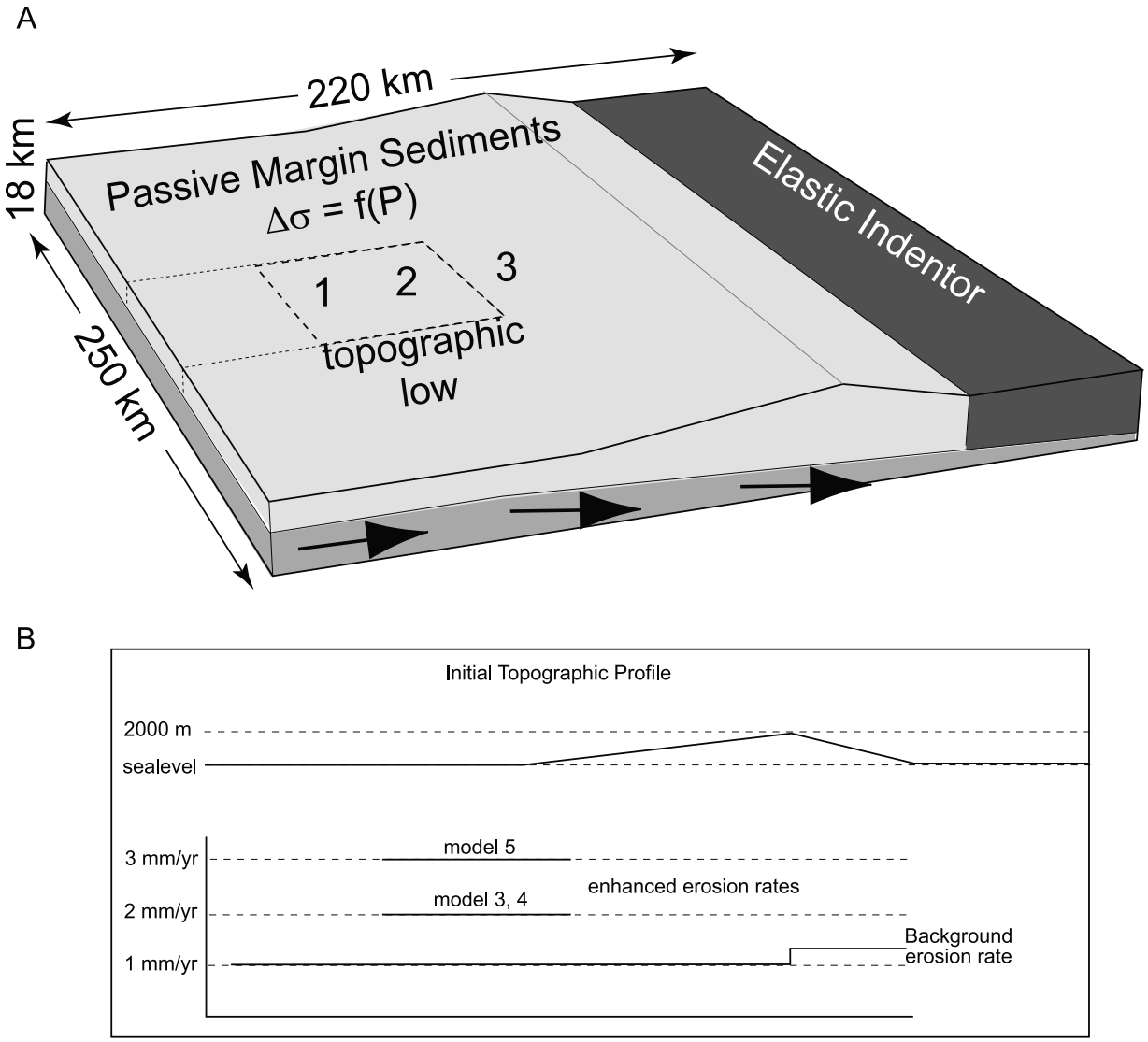

Figure 2. (a) Model geometry, material properties, and boundary conditions. Black arrows show the imposed tectonic velocity conditions. The bold dashed line outlines the region of the model "hole." In some models this is a preexisting hole; in others, this is a region of more intense erosion. The lighter dashed line outlines the region of weaker, less dense sediments included in some models. Numbers refer to history locations referred to in the text. We refer to the models in the geographic reference frame shown here: north–south is along strike, east is the inboard (or hinterland), and west is the outboard (or foreland). See text for details of individual models. (b) Initial topographic profile through the models and location of the variable erosion conditions imposed upon the models.

for the governing force and velocity equations using a modified Lagrangian technique that allows large strains, spatially and temporally varied erosion and also permits analysis of nonlinearities that arise in solution of the equations [*Cundall and Board*, 1988]. Materials are represented by polyhedral elements within a three-dimensional grid that uses an explicit, time-marching solution scheme and a form of dynamic relaxation. Each element behaves according to a prescribed linear or nonlinear stress/strain law in response to applied forces or boundary restraints. The constitutive relationships used in the models include elastic and nonassociated elastic-plastic (Mohr-Coulomb and Von Mises criteria [*Vermeer and de Borst*, 1984]).

[18] As with all numerical modeling packages FLAC^{3D} has advantages and disadvantages. It is a fully three-dimensional code and thus we can investigate both along- and across-strike features. A significant disadvantage is that

Table 1. Models and Properties

Model	ϕ_{eff}	$\phi_{b,eff}$	Weaker Region, ϕ_{eff}	Background Erosion (mm/a)	Enhanced Erosion (mm/a)
0	16°	5°	—	1/1.3	—
1	16°	5°	—	1/1.3	—
2	16°	5°	14°	1/1.3	—
3	16°	5°	—	1/1.3	2
4	16°	5°	14°	1/1.3	2
5	16°	5°	14°	1/1.3	3
6	16°	5°	14°	1/1.3	3 reduced to 0.5

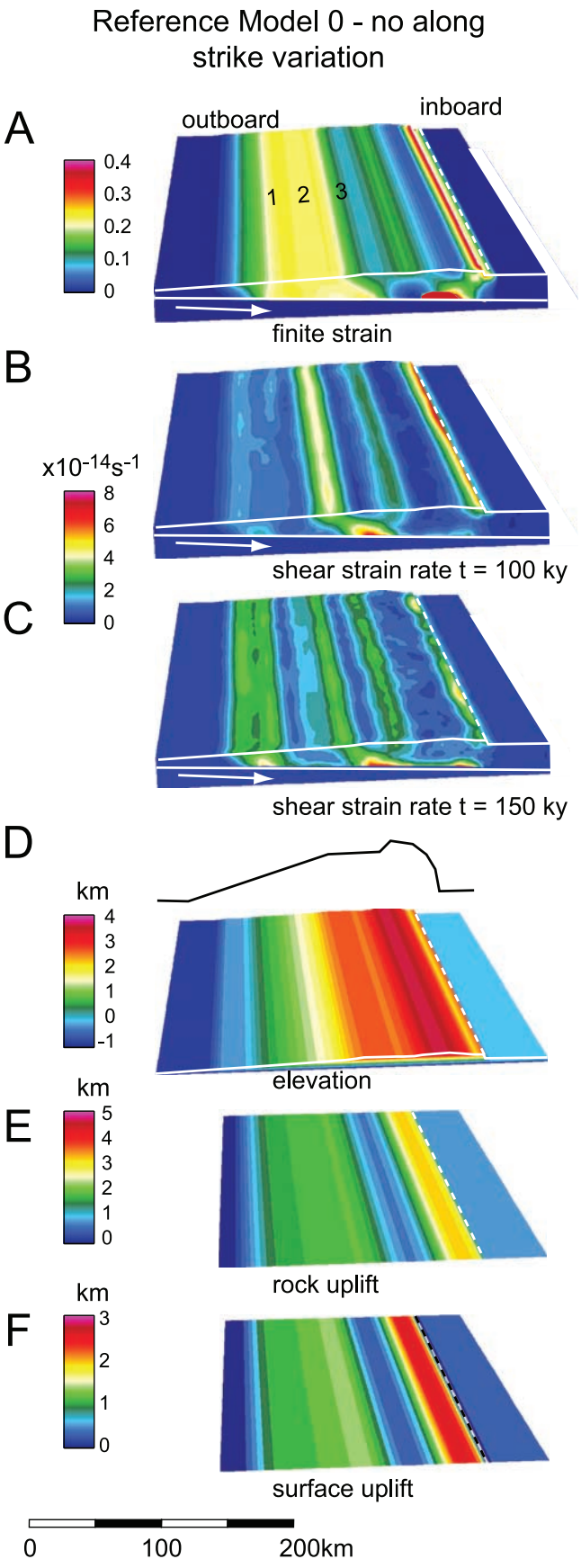

we are unable to regrid the models and thus are limited in how much strain our models can sustain. In general the models presented here were run to ~9% strain before numerical instabilities arising from distorted geometries caused the model runs to crash. While running the models, we monitor unbalanced forces which remain at a small fraction of the internal forces while the model is stable. The unbalanced forces increase rapidly as the stability of the model geometry reduces and we stop our models before this occurs. We ran all models to the same point and stopped them ~50 ka (model years) before they crashed, thus our solutions are not affected by the final numerical instabilities. With an input velocity of 20 mm/a and a 200-km-long model space, this allows us a runtime of just over 600 ka. The resolution of the models is 5 km in x and y and 2 km in the z direction. The model time step is 10 years. At the beginning of the models, the external controls (velocity and erosion) are imposed and the model is allowed to settle (reduction in unbalanced force) before analysis begins.

[19] We will describe a series of progressively more complex models which initially incorporate one of the following variables; a preexisting region of lower average topography in the wedge, a variation in strength or an erosional boundary condition. We then run models which consider both variation in strength and erosion. The models are run this way in order to document the individual effects before considering models in which effects may be either competing or enhancing each other. We do not intend that all of these models are realistic. Some are end-members and are unlikely to occur in nature, particularly the model that contains a preexisting hole. However, end-member models allow us to observe the response to a simple system and are thus a useful starting point.

4. Results

[20] In the following description of the results, three regions of lower elevation are described, two coinciding with the region shown as the initial hole or region of weaker rocks in Figure 2 and a third closer to the main divide. For clarity these will be referred to in the following manner (see Figure 2). Locality 1 refers to the left-hand half of the initial hole. Locality 2 refers to the right-hand half of the initial hole. Locality 3 refers to the region just to the right of locality 2. Locality 3 is not subjected to enhanced erosion nor does it contain the extra thickness of weaker rocks.

4.1. Reference Model With No Variation Along Strike (Model 0)

[21] Without any variation in topography, material properties or erosion rate along strike, the 3-D two-sided

Figure 3. Reference model results at the end of the model runtime. All results are invariant along strike. Numbers refer to history locations referred to in the text. (a) Shear strain. Strain is highest at the edge of the inboard, against the indentor, and in the outboard region. (b and c) Two snapshots of shear strain rate. Green to red shows region of higher strain rate. The locus of deformation within the foreland shifts between (d) elevation showing a constant taper, (e) rock uplift, and (f) surface uplift.

wedge develops exactly as the equivalent 2-D two-sided wedge described often in the literature [e.g., *Koons*, 1990; *Beaumont et al.*, 1992; *Willett et al.*, 2003; *Hoth et al.*, 2006, 2007]. The resolution of our 3-D models is necessarily coarser than that of most analog and 2-D numerical models and thus we are unable to model the actual thrust spacing (i.e., that observed in the field) in detail. However, we are confident that by examining a combination of instantaneous (e.g., shear strain rate) and cumulative (e.g., shear strain) parameters, our models can capture the overall pattern of deformation within a 3-D wedge at scales of >10 km [*Moresi et al.*, 2006]. That is, we can predict the location of the range front to within 10 km, but we cannot predict the distance between the range front fault and the previously active thrust fault.

[22] Strain in this model is concentrated against the indentor and in the outboard wedge (Figure 3a). In the foreland or outboard region, deformation is spread over approximately 70 km, inboard from the current range front (Figure 3a). Note that deformation in these models remains continuous and these individual shear zones are not associated with discrete frictional surfaces. The two snapshots of shear strain rate show that at any one point in time, deformation is more focused and occurs along a number of thrusts (Figures 3b and 3c and Figure S1 in the auxiliary material).[1] In the first snapshot shown (100 ka), an active thrust is located in the central foreland, with a back thrust and a small amount of strain is being taken up at the leading edge of the foreland (Figure 3b). In the second snapshot (150 ka), several thrusts within the foreland are active, including the range front (Figure 3c). The most active foreland thrust shifts with time in a way similar to 2-D discrete element [*Naylor and Sinclair*, 2007] and analog models [*Hoth et al.*, 2007]. Elevation, rock uplift and surface uplift are all invariant along strike (Figures 3d, 3e, and 3f).

4.1.1. Strength of the Décollement

[23] If the strength of the décollement is varied, the form of the wedge changes. A weak décollement causes deformation to occur along it rather than in the wedge, resulting in a flatter wedge. A strong décollement causes deformation to occur in the wedge rather than along the décollement, resulting in a steeper wedge.

4.1.2. Strength of the Wedge Material

[24] Increasing the strength of the wedge makes the décollement comparatively weaker, thus deformation is be spread out through the wedge resulting in a flatter wedge. Decreasing the strength of the wedge makes the décollement comparatively stronger, resulting in a steeper wedge.

4.2. Effects of a Preexisting Hole (Model 1)

[25] Incorporation of a preexisting hole or depocenter into the outboard of the orogen causes the wedge to back step and to fill in the hole (Figure 4a). This model has an initial 1000 m elevation difference between the hole (localities 1–2) and the surrounding regions. Rock uplift is focused into the right-hand half of the hole (locality 2) causing the highest surface uplift in the outboard region of the thrust belt. The region inboard of the hole (locality 3) has lower rock and surface uplift rates than elsewhere and this results in a region of lower elevation stepping back into the orogen. The resulting elevation plot shows a region of lower topography (locality 3) on the order of 1 km deep located ~50 km inboard of the original hole (localities 1–2, shown by the dashed box) after half a million years of model runtime. Rock uplift is focused into the original hole (localities 1–2). This deprives the adjacent region (locality 3) of material to build up the wedge relative to areas along strike.

4.3. Variation in Material Properties Within the Wedge (Model 2)

[26] Inclusion of a region of weaker or stronger material within the wedge affects the form of the wedge in a twofold manner. If the material is weaker, the wedge responds by increased deformation relative to the base and thus strain will be distributed through the weaker wedge rather than along the décollement, increasing α, the surface taper of the weaker region [*Dahlen*, 1984]. Stronger material closer to the indentor does not deform as much as it would in a uniform wedge because deformation is concentrated in the weaker material. A reduction in the density of the material fill has a similar effect. Because the wedge is made up of a pressure-dependent material, its strength at any particular depth is a function of the mass of material overlying it. If the density is decreased, it requires a greater mass of material to build up above it, before strain is transferred onto the décollement. We see these affects in model 2 where uplift is focused into weaker, less dense material (Figure 5b). The presence of weaker material leads to steeper average orogen slopes and high topography (Figure 4b). This model produces a region of lower topography within the wedge behind the weaker material (locality 3). Locality 3 is on the order of 400 m lower than the area along strike after a model runtime of 600 ka.

4.4. Accelerated Erosion Within the Wedge (Model 3)

[27] In model 3, the erosion rate is greater over a 50 x 50 km region, with 2 mm/a erosion rather than the background rate of 1 mm/a. A region of lower elevation develops as a result of the enhanced erosion (Figure 4c, locality 2). Localities 2–3 are ~800 m lower than the area along strike after a model runtime of 600 ka. Rock uplift in the region of enhanced erosion is enhanced but surface uplift is depressed (Figures 4c and 5c).

4.5. Accelerated Erosion and Variation in Material Properties Within the Wedge (Models 4, 5, and 6)

[28] The final three models combine the effects of material variations along strike with enhanced erosion.

4.5.1. Enhanced Erosion Rate of 2 mm/a (Model 4)

[29] The combination of more rapid erosion and a weaker material focuses rock and surface uplift into the region being eroded. The area of lower elevation that develops at locality 3 (behind the eroded region) is deeper than in model 3 (200 m in model 3, 4–600 m in model 4) as a result of the variation in material properties. The weaker material deforms more readily, thus the material behind it does not deform as much, and thus is not uplifted as much (Figure 4d).

4.5.2. Enhanced Erosion Rate of 3 mm/a (Model 5)

[30] An increase in erosion rate from 2 to 3 mm/a also creates a significant region of lower elevation within the

[1] Auxiliary materials are available in the HTML. doi:10.1029/2008JB005708.

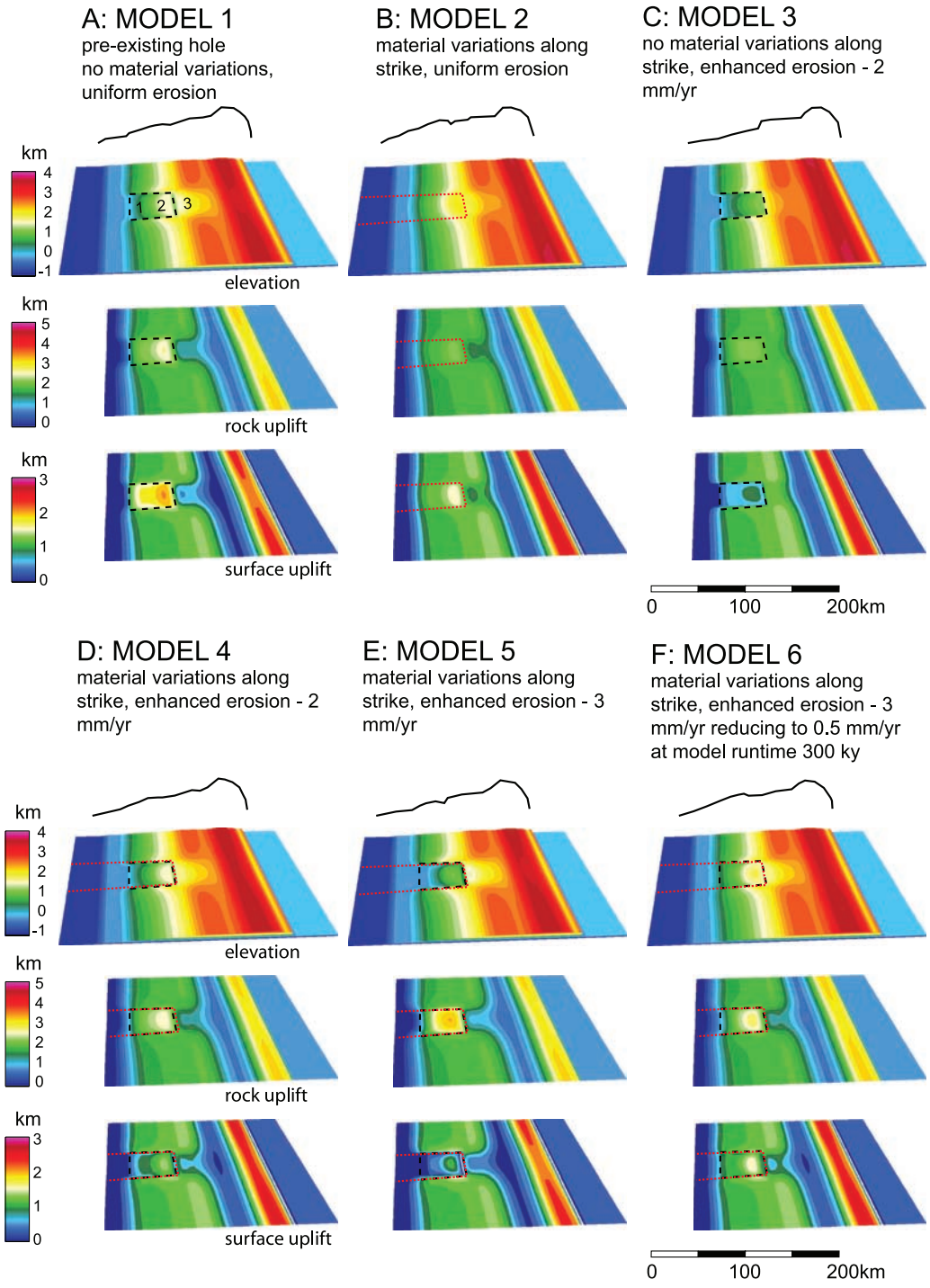

Figure 4. Contour plots showing elevation, rock uplift, and surface uplift (km) at the end of the model runtime for six of the models. Black dashed box represents preexisting hole in Figure 4a and region of enhanced erosion in Figures 4c, 4d, 4e, and 4f. Red dashed box represents region of different material properties in Figures 4b, 4d, 4e, and 4f. Numbers refer to history locations referred to in the text. (a) Model 1 with a preexisting hole and no focused erosion. (b) Model 2 with weaker, less dense material and no focused erosion. (c) Model 3 with uniform material and enhanced erosion (2 mm/a). (d) Model 4 which combines models 2 and 3. (e) Model 5, same as for model 4 but with faster erosion. (f) Model 6, same as for model 5 but erosion is reduced in the later stages of the model runtime. See text for details of the model results.

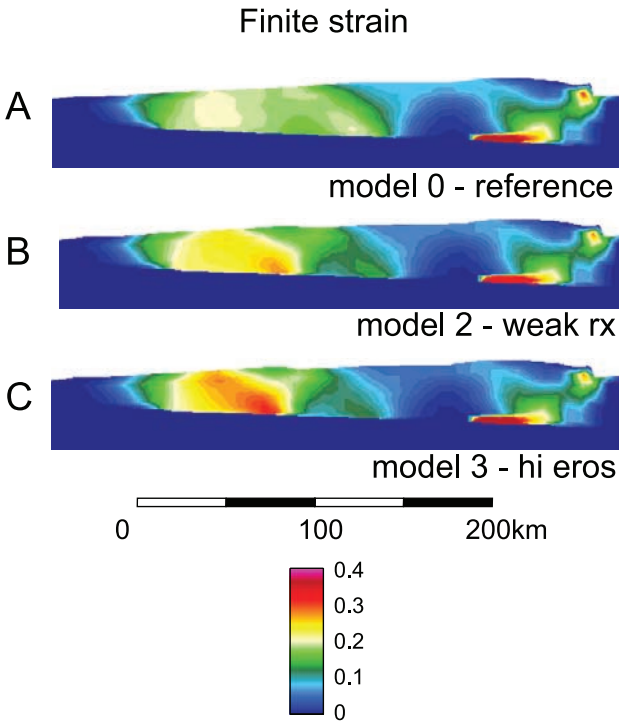

Figure 5. Contour plots of finite strain for the reference model, model 2, and model 3. Strain is focused into the region of weaker material in model 2 and into the region with a higher erosion (hi eros) rate in model 3; rx, rock.

model (Figure 4e). The region of lower elevation can be divided into three parts, the left-hand section has low uplift rates, low deformation rates and results largely from the imposition of high erosion rates (locality 1). The central portion is the most active with high rates of rock uplift, high deformation rates and its elevation results from a balance between uplift and erosion (locality 2). The right-hand portion of the topographic low is not being actively eroded and its lower elevation is a result of material being focused away from it and into the central portion (locality 3). The range front in this model steps inboard adjacent to the eroded region (Figure 4e). Compared to the reference model, strain is concentrated beneath the region of enhanced erosion rate (Figure 5).

4.5.3. Enhanced Erosion Rate of 3 mm/a Reduced to 0.5 mm/a (Model 6)

[31] In this model, the erosion rate is instantly reduced from 3 mm/a to 0.5 mm/a at 300 ka model time. The form of this model is similar to the previous, however, the elevation difference between the hole and surrounding regions is less and the amount of surface uplift is significantly higher (Figure 4f). When the erosion rate is decreased, material moving into the region of lower topography is no longer removed by erosion and the wedge begins to build itself up again, resulting in high surface uplift into the hole (similar to model 1).

4.5.4. Size of the Region of Enhanced Erosion

[32] Enhanced erosion in these models affects the elevation, rock and surface uplift of the region subjected to higher erosion rates but it also affects other areas. In these models, the scale over which this interaction occurs is related to the size of the eroding area. As these models are orthogonal, deformation along strike is largely unaffected but deformation across strike appears to be affected to approximately the distance of the perturbation (Figure S2). That is, for a region of ~30 km subjected to enhanced erosion, the model shows that material ~30 km away from that region is affected. For oblique deformation, we would expect a similar result, that is, we would expect material ~30 km along strike to be affected by the enhanced erosion.

4.6. Comparing Models Using Histories of Elevation, Uplift, and Strain

[33] Elevation, vertical velocity, vertical displacement, surface displacement, and shear strain rate have been recorded at three locations (shown in Figure 2) in the models such that we can compare the evolution of the model orogen with time (Figures 6 and 7). Uplift velocity at all three locations varies cyclically from near zero at times to as high as 18 mm/a (Figure 6) as one thrust and then another accommodates a higher proportion of the shortening. If we take locality 2 (back of hole) in the reference model (black line) as an example, uplift at this point is initially slow (~1–2 mm/a), then there is a phase of rapid uplift (~8 mm/a) followed by nearly zero uplift followed by another phase of more rapid uplift (Figure 6b). These peaks in rock uplift correspond to periods of accelerated increase in elevation (Figure 7b). These cycles appear to last on the order of 15–200,000 model years. Over one cycle the uplift rate averages ~3 mm/a. These results are compatible with observations from discrete element models [*Naylor and Sinclair*, 2007] and analog experiments [*Hoth et al.*, 2007]. *Hoth et al.* [2007] showed that thrusting occurs in cycles with different thrusts active at different stages through a particular cycle. We note that this behavior is unlikely to be resolved using fission track or even helium thermochronology in active thrust belts, given the short timescales at which it is likely to occur [e.g., *Lock*, 2007].

[34] These cycles are affected by the imposed erosion rate. For locality 2 we plot model 1 (preexisting hole) and model 5 (high imposed erosion rate). In both cases a thrust cycle uplifts this point earlier than in the reference model. The highest rock uplift rate for the peak of the first thrust cycle also increases relative to the reference model. The increased erosion rate (or change in material properties) also affects the region outside of the imposed change. Locality 3 is outside both regions yet is strongly affected with a reduction in its elevation in all models, most noticeably in model 1 with the preexisting hole and in model 5 with the highest erosion rates within the eroding region. Material in the reference model that was uplifted at locality 3 is instead being uplifted at locality 2 to replace material missing or removed from the eroding region.

[35] Model 6 diverges from model 5 when the erosion rate at localities 1–2 is reduced from 3 mm/a to 0.5 mm/a at 300 ka model time (Figures 6a, 6d, and 7). The model responds almost instantly at all localities (Figure 7). At locality 1 the rock uplift rate decreases slightly but combined with the drastic reduction in the amount of material being removed, both surface uplift and elevation increase dramatically (Figures 6 and 7). Localities 2–3 respond similarly. *Hoth et al.* [2006] also found that the analog

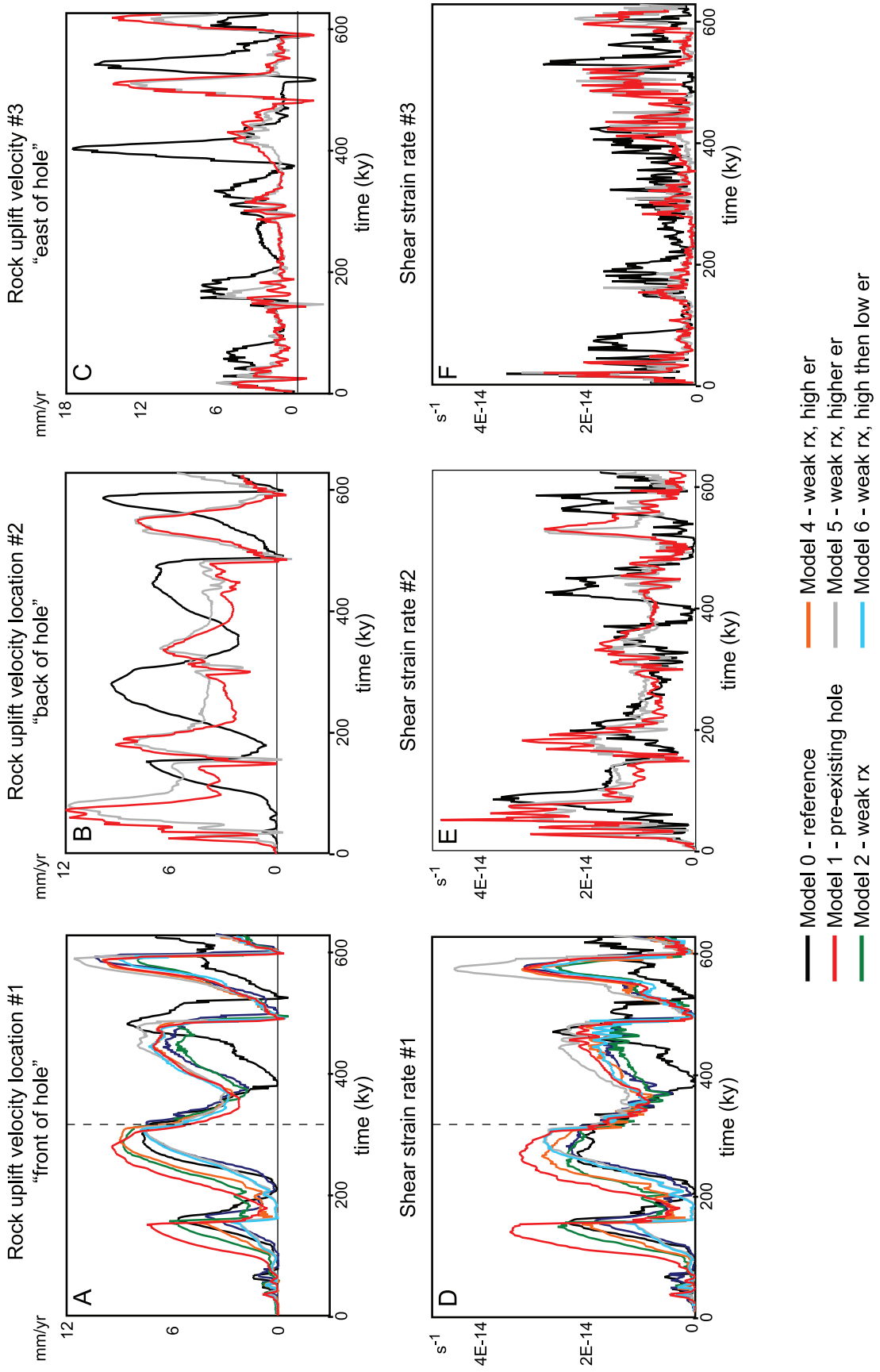

Figure 6. History plots of rock uplift velocity and shear strain rate for the three locations shown in Figure 2. For clarity only models 0, 1, and 5 are shown for locations 2 and 3. The vertical dashed line marks the time at which the erosion rate (er) in model 3f is reduced from 3 to 0.5 mm/a at 300 ka. Note that the scales change between localities. See the text for details.

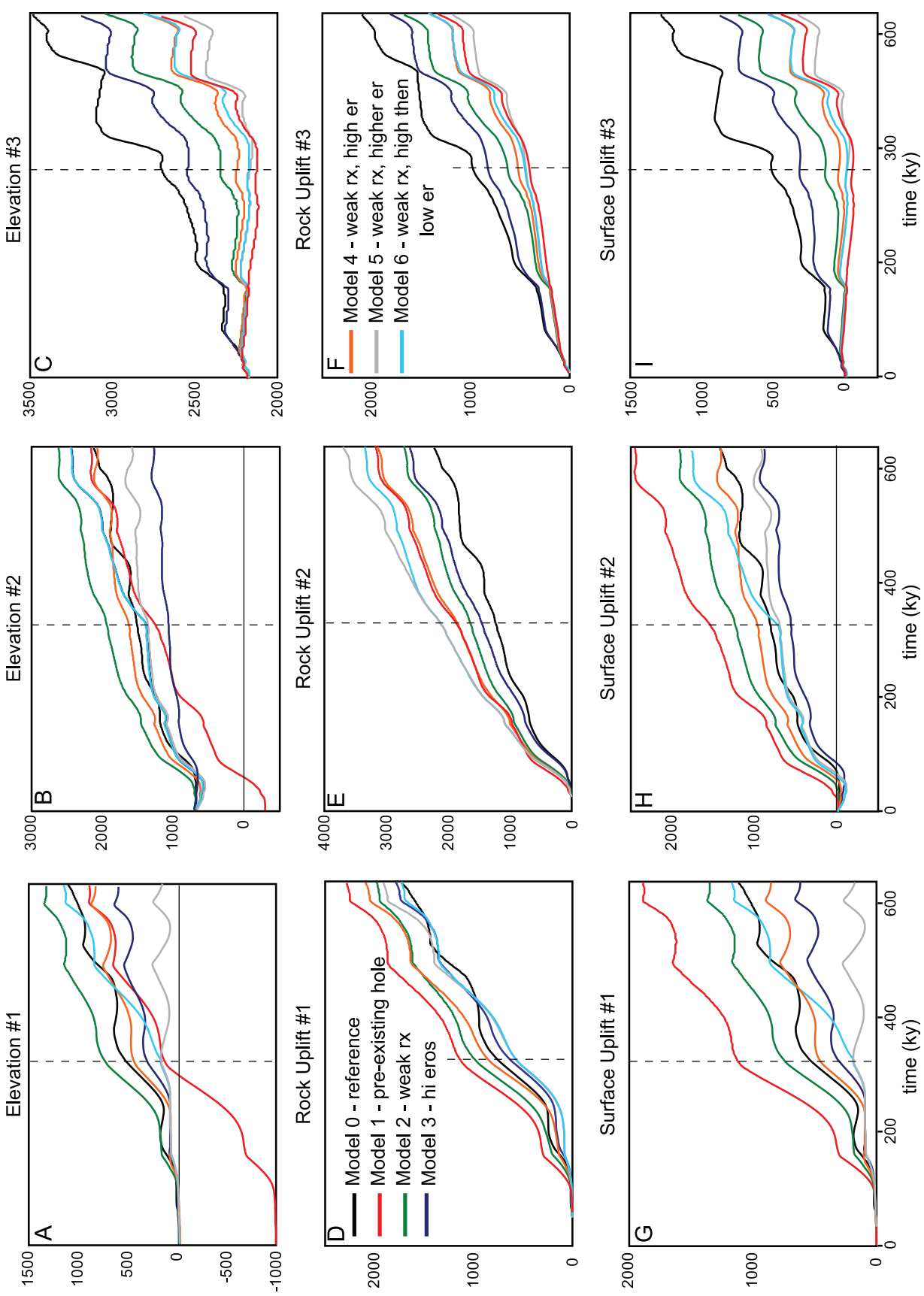
A
Elevation #1
B
Elevation #2
C
Elevation #3
D
Rock Uplift #1
Model 0 - reference
Model 1 - pre-existing hole
Model 2 - weak rx
Model 3 - hi eros
E
Rock Uplift #2
F
Rock Uplift #3
Model 4 - weak rx, high er
Model 5 - weak rx, higher er
Model 6 - weak rx, high then low er
G
Surface Uplift #1
H
Surface Uplift #2
I
Surface Uplift #3
time (ky)

Figure 7

models responded very quickly to a change in the erosional regime.

5. Discussion

[36] In any active orogen, a complete set of observations, required to allow a total description of the deforming region, are never available. Too many degrees of freedom exist to completely describe the observed deformation in terms of the material rheology and the imposed boundary conditions. Active orogens that exhibit regional along-strike variation in strain patterns with little change in the boundary conditions can reduce the degrees of freedom, however, allowing limits to be placed on the controlling interplay between rheology and erosion (e.g., Salt Ranges, Pakistan [*Davis and Lillie*, 1994]; North Island, New Zealand [*Upton et al.*, 2003a]; and South Island, New Zealand [*Upton et al.*, 2009]).

5.1. Implications for the Form of a Three-Dimensional Wedge With Variable Material Properties and Erosion Rates

[37] Our models offer insight into the response of a compressive wedge to coupled erosion and strain (Figure 8). The effect on rock uplift, surface uplift and topography of along-strike variation within the three-dimensional wedge are not always intuitive and we discuss these below.

5.1.1. Preexisting "Hole"

[38] While a preexisting hole is not a realistic model, it is useful to study as an end-member case for comparison with the other models we have run. The effect of a preexisting hole being incorporated into the model orogen is the development of an area of lower topography further inboard into the model orogen (model 1; locality 3, Figures 4a and 8b). Both rock and surface uplift are focused into the original hole as the wedge attempts to rebuild itself. This has the effect of reducing the amount of material available to build the orogen in a inboard direction, reducing both rock and surface uplift, and thus elevation, inboard of the original hole.

5.1.2. Incorporation of Weaker/Less Dense Material Into the Wedge

[39] The inclusion of weaker/less dense material into the wedge has the effect of building up the wedge at that point and resulting in a decrease in strain and rock uplift further inboard into the orogen (Figures 4b and 8c). Stronger material that lies in the adjacent inboard region does not deform as much because deformation is forced into the weaker material. By having variable material properties within a wedge, only some of the wedge will be close to failure at any one point in time. The stronger material within the wedge does not always reach criticality during the deformation, because stress buildup will lead to failure within the weaker material first.

5.1.3. Enhanced Erosion Rates

[40] Focused erosion, if it is rapid enough, will produce a topographic depression within the fold and thrust belt, even in a region where weaker rocks are being uplifted more rapidly. This implies that an orogen is capable of maintaining a region of lower elevation, in spite of accelerated rock uplift, given boundary conditions similar to model 5 (Figures 4e and 8f). Material is focused into the rapidly eroding region to replace that removed, thus depriving the region inboard of material. The result is a three-level, or stepped, region of lower topography, each with distinct characteristics. Deeper within the orogen, behind the region of high erosion, is the inboard part of the hole (locality 3). Here rock uplift and the amount of deformation are both reduced. Beneath the region of focused erosion, the central part of the hole, uplift rates are much higher and shear strain is focused here (locality 2). A dramatic change in elevation develops at the boundary between these two levels. A reduction in the erosion rate (model 6; Figures 4f and 8g) allows the lower level of the hole to begin to build back up again. Rock and surface uplift are focused into the lower level, bringing it up to the level of the eastern part of the hole. Our model was unable to continue beyond this point, but continued deformation would continue to build up the regions of lower topography, filling in the foreland part first. Erosion in our models is prescribed as a fixed rate. The use of a real denudation law, which usually relate the rate of erosion to some expression of the topographic slope, would likely subdue the effects we observe in these models. In particular, the distinct sequence of three low topography regions maybe more gradual.

5.1.4. Scale of Interactions

[41] These results suggest that an orogen with boundary conditions similar to those modeled here may be driven by strong coupling between erosion and strain. With appropriate data available (well dated older structures, growth strata and higher resolution geothermometry), we should be able to see activity shifting as a result of a change in the erosional conditions over timescales of 10^4–10^5 years and spatial scales comparable to the scale of the erosional perturbation. That is, if the region of enhanced erosion is 30 km in length, up to about 30 km from the edge of the imposed erosion condition we would expect the strain pattern to be perturbed.

5.1.5. Effect of No Isostatic Compensation

[42] Our models do not simulate isostatic compensation and thus elevations are exaggerated. If included, removal of material by erosion would cause an isostatic rebound, however, the rebound would also increase the rate of rock uplift into the eroding area. Thus, while the topographic signal seen in the models would be subdued by including isostatic compensation, the rock uplift signal would be enhanced. The effect of the isostatic compensation will occur over a broader scale than the effects of the localized erosion, so that on the small scales we are interested in, isostatic effects will be diffuse compared with the response of the wedge.

Figure 7. History plots of elevation, total rock uplift, and total surface uplift for all models at the three locations shown in Figure 2. Location 1 is on the western edge of the "hole," location 2 in on the eastern edge of the "hole," and location 3 is to the inboard of the "hole." The reference model with no along-strike variation is shown in black and can be used to infer the along-strike values for the other models. The vertical dashed line marks the time at which the erosion rate in model 3f is reduced from 3 to 0.5 mm/a at 300 ka. Note that the scales change between localities. See the text for details.

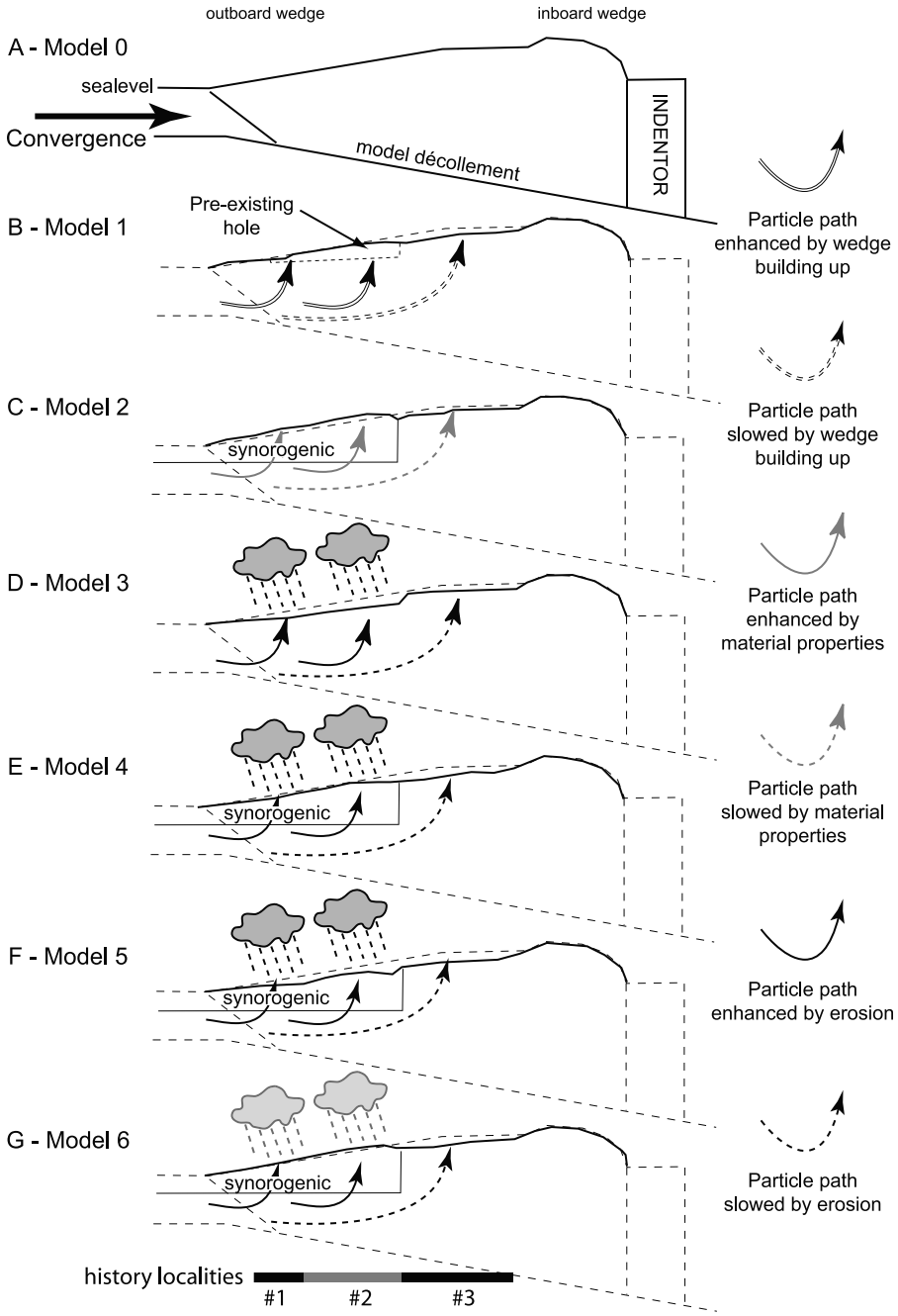

Figure 8. Synopsis of results. Schematic outline (vertical exaggeration ~3X) of the model wedge for different material properties and erosion schemes. The dashed lines in Figures 8b–8g are the outline of the reference model. (a) Reference model. (b) Model with a preexisting hole. (c) Weaker, less dense Plio-Pleistocene sediments in the region of interest. (d) Uniform wedge with enhanced erosion of 2 mm/a. (e) Weaker, less dense Plio-Pleistocene sediments with enhanced erosion of 2 mm/a. (f) Weaker, less dense Plio-Pleistocene sediments with enhanced erosion of 3 mm/a. (g) Weaker, less dense Plio-Pleistocene sediments with enhanced erosion of 3 mm/a reducing to 0.5 mm/a.

5.2. Thrust Cycling Within the Models and Nature

[43] Tracking strain rate, rock uplift rates and other parameters through time reveals that the actively deforming region of the model changes with time at short spatial and temporal scales (Figure 6 and Figures S1, S3, S4, and S5). Over the runtime of the model, the whole outboard region of the model deforms. At any one time activity may be concentrated onto one or more structures. This affect is less pronounced at locality 2 for models 1 and 5 which have a nonzero rock uplift velocity for almost all of the model runtime (Figure 6b). This is because deformation is focused into the region of locality 2 by either filling of the preexisting hole or the enhanced erosion and thus these structures are almost always active, unlike in the reference

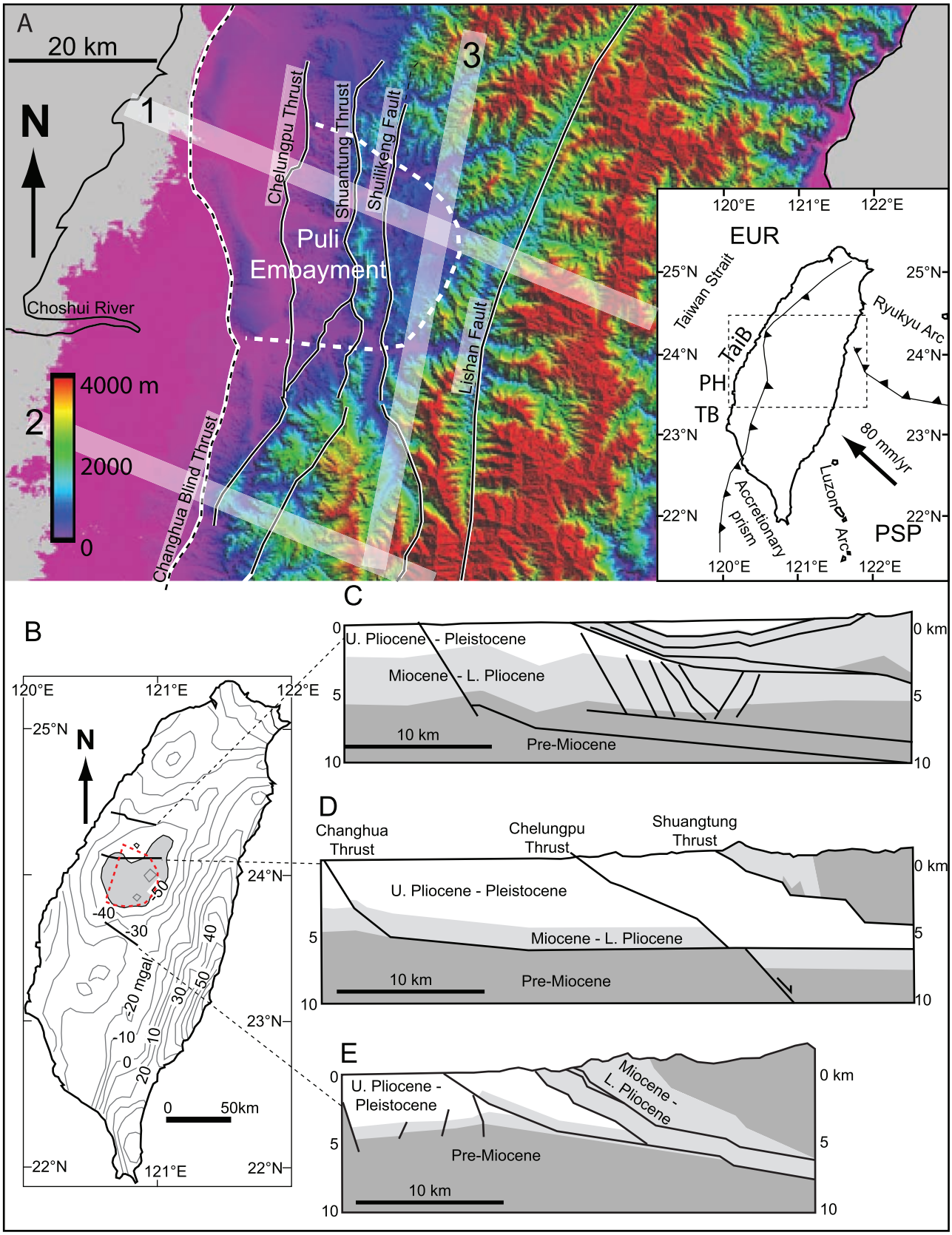
A
20 km
N
1
2
3
4000 m
2000
0
Chelungpu Thrust
Shuantung Thrust
Shuilikeng Fault
Lishan Fault
Changhua Blind Thrust
Puli
Empayment
Choshui River
120°E
121°E
122°E
EUR
25°N
24°N
23°N
22°N
Taiwan Strait
Ryukyu Arc
TaiB
PH
TB
80 mm/yr
Accretionary prism
Luzon Arc
PSP
B
C
D
E
50km
≤20 mgal
U. Pliocene - Pleistocene
Miocene - L. Pliocene
Pre-Miocene
10 km
0 km
Changhua Thrust
Chelungpu Thrust
Shuangtung Thrust
Miocene - L. Pliocene

Figure 9

model where these structures turn off and on more regularly (Figures S1 and S5).

[44] The critical wedge approximation assumes that the whole wedge is always at failure and responds instantaneous to any perturbations by a change in surface taper, thus maintaining criticality [*Davis et al.*, 1983]. However, neither model nor real wedges are truly critical and they likely exhibit more complex behavior [e.g., *Hoth et al.*, 2006, 2007; *Naylor and Sinclair*, 2007]. In the models presented here and in analog [e.g., *Hoth et al.*, 2006, 2007] and discrete element models [*Naylor and Sinclair*, 2007] the wedge grows by the accretion of material into frontal thrust.

[45] Characterizing the long-term temporal variability of slip rate on single thrusts within natural fold and thrust belts is likely to be difficult, but some examples do exist. Cosmogenic ^{10}Be dating along the Asku Fault (Tian Shan, China) reveals a record of activity followed by a long quiescence (at least 7.5 ka) and recent activity over the past 5 ka [*Hubert-Ferrari et al.*, 2005]. *Masaferro et al.* [2002] showed that the Neogene-Quaternary growth of the Santaren anticline (Cuban fold and thrust belt) is characterized by several tectonic uplift pulses of different duration and intensity, interrupted by periods of variable duration in which no fold growth occurred. The Pyrenees show a punctuated pattern of exhumation [*Sinclair et al.*, 2005]. Given these examples and results from both numerical [*Naylor and Sinclair*, 2007; this study] and analog [*Hoth et al.*, 2006, 2007] modeling, it appears that transient accommodation of strain may be a rather common process. Thus caution should be used when extrapolating slip rates from different temporal scales, particularly within the outboard region of a two-sided wedge [*Hoth et al.*, 2007].

[46] A change in the erosional condition (model 5 versus model 6) results almost immediately in an increase in the amount of surface uplift, elevation and the strain rate (Figures 6, 7, and S1). The orogen thus appears to respond almost instantly to a change in the external forcing of the system. *Hoth et al.* [2006] also found that the analog models responded very quickly to a change in the erosional regime. In nature, it is unlikely that erosion rates vary as abruptly in our models and thus some lag period in erosion rates may exist from one climate regime to another. If this is the case, then we would expect a more gradual response in nature because of the more gradual change in the erosion rates.

5.3. The Puli Embayment, Taiwan: An Example?

[47] Our numerical study was partially motivated by the existence of the Puli Embayment, a 50-km-wide topographic low within the western central Taiwanese thrust belt, which has been recognized as a potentially anomalous region of west central Taiwan [*Mueller et al.*, 2001, 2002; *Upton et al.*, 2003b]. We wondered if the presence of the embayment could be reflecting a signal of surface processes. Taiwan lies in the path of strong typhoons, averaging four per year, has a subtropical climate and a mean precipitation of 2.5 m/a [*Wu and Kuo*, 1999]. High rainfall and relief, easily eroded sediments or their weakly metamorphosed equivalents all contribute to high erosion rates recorded in Taiwan [e.g., *Willett et al.*, 2003; *Dadson et al.*, 2003; *Fuller et al.*, 2006].

[48] The Puli Embayment is about 1500 m lower in average elevation than the surrounding areas in the thrust belt (Figures 9a and 10). The Puli region exposes young piggyback basin deposits [*Powell et al.*, 2003] that are deformed by active folds $\sim$40–50 km east of the leading edge of the thrust belt [*Mueller et al.*, 2001, 2002]. Thrust sheets in the Puli region trend NNE, and extend across the bowl-shaped region of lower topography (Figure 9a). The area of lower topography around the Puli region also coincides with the edges of a large ($\sim$50 mGal) negative gravity anomaly (Figure 9b) [*Yeh and Yen*, 1992]. The basal décollement beneath the Puli region occurs within the Pliocene Chinshui Shale [*Yue et al.*, 2005, 2009]. The depth of the décollement beneath Puli is 5.5–6 km and it dips east at $\sim$3° [*Yue et al.*, 2005, 2009]. *Suppe* [2007] suggests that the décollement is very weak with $\mu = 0.07–0.11$, based on the assumption of a relatively strong wedge.

[49] The Taiwanese foreland, onshore and offshore, contains numerous Tertiary basins [*Mouthereau et al.*, 2002]. Opening of the South China Sea during the Oligocene to early Miocene stretched the lithosphere and formed early Paleogene basins which trend northeast [*Mouthereau et al.*, 2002]. Stretching continued in the Neogene but with a different orientation and these new basins, which trend northwest, cut across the older structures [*Mouthereau et al.*, 2002]. Following development of the Taiwan orogen over the last 5 Ma, the foredeep basins have been superimposed onto the precollisional basins, resulting in large differences in the thickness of Plio-Pleistocene sediment coming into the orogen [*Mouthereau et al.*, 2002].

[50] The differences in sediment thickness coming in the orogen described above may contribute to the resulting topographic profile of the Puli Embayment. Thrust sheets in the Puli area are capped by a thicker sequence of synorogenic fill [*Yang et al.*, 2007]. Interpreted seismic profiles across the Puli region suggest the combined thickness of synorogenic foreland basin fill (Plio-Pleistocene) is $\sim$5 km thick (Figure 9c). In contrast, sections located to the north and south of the Puli Region exhibit thinner sequences of synorogenic fill, capping thrust sheets accreted into the orogen [*Yang et al.*, 2007] (Figure 9c). Because of the lack of induration of these rocks compared to the Miocene

Figure 9. (a) Digital elevation model of central Taiwan showing the Puli Embayment, a region of lower elevation within the Western Foothills and the major faults. White boxes show the areas of swath topographic profiles shown in Figure 10. Inset shows the tectonic setting of Taiwan. EUR, Eurasian Plate; PSP, Philippine Sea Plate; PH, Peikang High; TB, Tainan Basin; TaiB, Taichung Basin. (b) Bouguer anomaly map of Taiwan [after *Yeh and Yen*, 1992]. The <−50 mGal anomaly (shaded) indicates a Pleistocene depocenter [*Mouthereau et al.*, 1999]. Dashed red line shows the location of the Puli Embayment. (c–e) Simplified geological sections from Chinese Petroleum Company (modified from *Yang et al.* [2007] with permission). Location of the sections shown in Figure 9b. Note the greater thickness of upper Pliocene–Pleistocene rocks along the middle section and that these extend to the east beneath the Shuangtung Thrust.

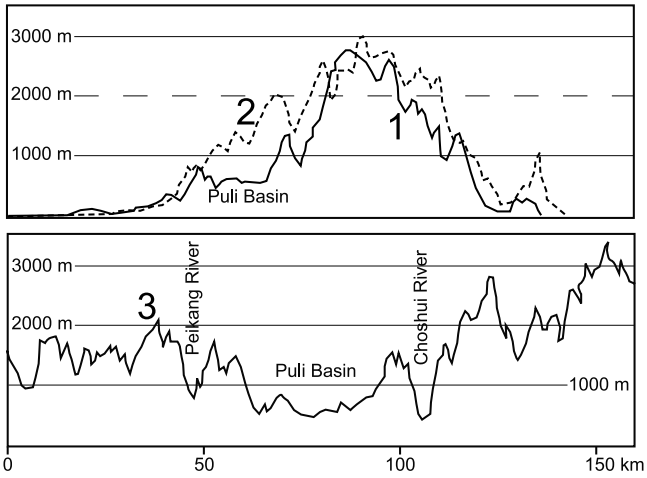

Figure 10. Three swath topographic profiles through central Taiwan. Profiles 1 and 2 run approximately east–west. The Puli Embayment is a prominent feature on profile 1. Profile 3 runs north–south through the Puli Embayment.

sandstone and shale underlying them, we suggest that not only are these rocks of the Plio-Pleistocene sediments slightly lower in density to those to the north and south but they may also be frictionally weaker. We suggest that lower topography in Puli may result from more rapid erosion of thicker sequences of synorogenic alluvial fill that capped thrust sheets accreted into this part of the thrust belt [*Mueller et al.*, 2006]. The age of strata exposed within and around the periphery of Puli indicates significant amounts of erosion; this is supported by published apatite fission track data [*Fuller et al.*, 2006] that argue for up to 5 km of exhumation consistent with the age and thickness of Tertiary strata exposed in the area.

[51] In the Puli region, deformation appears to be spread over a 50-km-wide region which incorporates four prominent faults. From east to west these are the Shuilikeng, the Shuangtung, the Chelungpu, and the Changhua blind thrust (Figure 9a). The two frontal thrusts, the Changhua and Chelungpu are clearly active and accommodate much of the current shortening at the leading edge of the belt [*Simoes et al.*, 2007a, 2007b; *Yue et al.*, 2009]. Activity on the Chelungpu thrust began 0.7–1.0 Ma and it has a total slip of ~14 km [*Yue et al.*, 2009]. The Changhua thrust is in a much earlier stage of development with only 1.7 km of displacement since its inception at ~62 ka [*Simoes et al.*, 2007a, 2007b; *Yue et al.*, 2009]. At least 12 km of displacement has taken place on the Shuangtung thrust [*Yue et al.*, 2005]. Its inception is estimated to have occurred prior to 1.1 Ma [*Simoes and Avouac*, 2006]. Geomorphic analysis suggests that the Shuangtung thrust is presently inactive [*Yue et al.*, 2009; *Yanites et al.*, 2007; B. J. Yanites et al., Channel dynamics in a critical wedge: Deformation, hydraulic geometry, and stream incision patterns along the Peikang River, Central Taiwan, paper presented at 2007 GSA Denver Annual Meeting, Geological Society of America, 28–31 October 2007], although deactivation may have occurred relatively recently [*Yue et al.*, 2009]. The oldest of these fault structures, the Shuilikeng, is also presently active, being an example of out-of-sequence thrusting [*Sung et al.*, 2000; *Powell et al.*, 2003; *Wilcox et al.*, 2007; *Yanites et al.*, 2007, B. J. Yanites et al., presented paper, 2007]. Fieldwork in the Puli region suggests that recent rock uplift and rapid incision are associated with the Shuilikeng thrust based on deformed terrace deposits in the central part of the basin [*Powell et al.*, 2003; *Wilcox et al.*, 2007] and in the Peikang River valley [*Yanites et al.*, 2007, B. J. Yanites et al., presented paper, 2007]. Uplift rates of ~5 mm/a are estimated from folding and incision rates upstream of the Shuilikeng Fault [*Wilcox et al.*, 2007; *Yanites et al.*, 2007, B. J. Yanites et al., presented paper, 2007].

5.4. Comparison of Models and the Puli Embayment

[52] The Puli region is striking for its low topography, apparent high rates of deformation [e.g., *Simoes et al.*, 2007a, 2007b; *Yue et al.*, 2009; *Powell et al.*, 2003; *Wilcox et al.*, 2007; *Yanites et al.*, 2007, B. J. Yanites et al., presented paper, 2007], high erosion rates [*Fuller et al.*, 2006] and out of sequence thrusting. We suggest that these features are at least partially a result of thicker, more erodible synorogenic sediments in the Puli region. Our models show that enhanced erosion within a region such as Puli will focus material into that region. They also show that a topographic low within an actively deforming wedge will tend to refill itself and will not be a long-term feature, unless material is continually removed by enhanced erosion. If the erosion rate is high enough, the topographic low can be maintained, even though rock uplift rates are enhanced. Our models also show that within a deforming wedge, deformation will shift between structures over time. This result has also been found in other modeling studies [e.g., *Hoth et al.*, 2006, 2007; *Naylor and Sinclair*, 2007]. In the Puli region we may see an example of a thrust fault being switched off (the Shuangtung) while another one has been switched back on (the Shuilikeng).

[53] Further testing is required to determine whether or not these models can explain some or all of the topographic and deformational characteristics of the Puli Embayment. This region has received considerable attention over the past decade, following the 1999 Chi-Chi earthquake. It is also more accessible than the mountainous regions to the north and south. Structural and geomorphic data as well as low-temperature geochronology from the areas to the north and south of the Puli Embayment are needed to quantify the differences in deformation style between the regions. If, as we suggest, variation in material properties and erosion rate are playing a role, then we would expect deformation to the north and south to be more localized in time and space.

6. Conclusions

[54] Along-strike variation in the topography of a compressive wedge implies variation in one or more of the parameters controlling rock uplift and erosion of the wedge. We have developed and run a series of three-dimensional mechanical models aimed at investigating how the form and kinematics of the outboard wedge responds to variations in initial topography, material properties and erosion rate. When a wedge is subcritical, either as a result of an initial topographic hole, the incorporation in the wedge of lower

density material or as a result of enhanced erosion, the wedge will focus material into that region in an attempt to rebuild the wedge to criticality. In doing so, the regions inboard are deprived of material, resulting in a new area that is subcritical and has lower topography. In our models, an imposed erosion rate of 3 mm/a (tectonic rate of 20 mm/a distributed across the model) was sufficient to produce and maintain a topographic depression within the outboard of the model. Material is focused into the eroded region and is withheld from the region inboard. This leads to the development of a stepped region of lower topography within the model.

[55] We recorded rock uplift, surface uplift and other parameters at three locations within the models. The uplift velocities at the locations monitored varied cyclically from near zero to ~3 times the average uplift rate. Over the runtime of the model, the whole outboard region deforms, however, the focus of active deformation shifts on short spatial and temporal scales. At any one time, activity may be concentrated onto more or more structures. These cycles last on the order of 15–200,000 model years. Our models, along with other numerical [*Naylor and Sinclair*, 2007] and analog models [*Hoth et al.*, 2006; 2007] and some well dated examples from active orogens [*Masaferro et al.*, 2002; *Hubert-Ferrari et al.*, 2005; *Sinclair et al.*, 2005], suggest that transient accommodation of strain may be common. Thus, caution should be applied when extrapolating long-term slip rates from varying temporal scales. The cycles observed respond rapidly to changes in the amount of erosion imposed. Our models suggest that orogens may be driven by remarkably strong coupling between erosion and strain, on temporal scales of 10^4–10^5 years and spatial scales comparable to the scale of the erosional perturbation.

[56] We compare our models to the Puli Embayment of west central Taiwan, a region of anomalous low topography and suggest that it presence may reflect the presence of weaker and more erodible sediments than those present along strike in the orogen. Inboard of the range front, deformed terraces and rapid incision rates imply that the Shuilikeng Thrust is active [*Powell et al.*, 2003; *Wilcox et al.*, 2007; *Yanites et al.*, 2007; B. J. Yanites et al., presented paper, 2007]. Our models suggest that removal of material from the Puli Embayment may be contributing to deformation stepping back to the basin, onto the Shuilikeng Thrust.

[57] **Acknowledgments.** Funding for this project was provided by the National Science Foundation to P. Upton (EAR0510051) and K. Mueller (EAR0510971). Perceptive comments by Doug Burbank, Stephane Dominguez, and two anonymous reviewers helped to clarify the manuscript. We thank Shao-Yi Huang, Ray Y. Chuang, Yu-Ting Kuo, and Kuo-Wei Shih for assistance in the field. Discussions with John Suppe, Peter O. Koons, Sean Willett, Jean Phillipe Avouac, Martine Simoes, Brian Yanites, Tarka Wilcox, and Lauren Powell are appreciated.

References

Avouac, J. P., and E. B. Burov (1996), Erosion as a driving mechanism of intracontinental mountain growth, *J. Geophys. Res.*, *101*, 17,747–17,769, doi:10.1029/96JB01344.

Beaumont, C., P. Fullsack, and J. Hamilton (1992), Erosional control of active compressional orogens, in *Thrust Tectonics*, edited by K. R. McClay, pp. 1–18, Chapman and Hall, New York.

Beaumont, C., S. Ellis, J. Hamilton, and P. Fullsack (1996), Mechanical model for subduction-collision tectonics of Alpine-type compressional orogens, *Geology*, *24*, 675–678, doi:10.1130/0091-7613(1996)024<0675:MMFSCT>2.3.CO;2.

Berger, A. L., and J. A. Spotila (2008), Denudation and deformation in a glaciated orogenic wedge: The St. Elias Orogen, Alaska, *Geology*, *36*, 523–526, doi:10.1130/G24883A.1.

Berger, A. L., et al. (2008), Quaternary tectonic response to intensified glacial erosion in an orogenic wedge, *Nat. Geosci.*, *1*, 793–799, doi:10.1038/ngeo334.

Bernet, M., Z. Massimiliano, J. I. Garver, M. T. Brandon, and J. A. Vance (2001), Steady-state exhumation of the European Alps, *Geology*, *29*, 35–38, doi:10.1130/0091-7613(2001)029<0035:SSEOTE>2.0.CO;2.

Burbank, D. W., A. E. Blythe, J. Putkonen, B. Pratt-Sitaula, E. Gabet, M. Oskin, A. Barros, and T. P. Ojha (2003), Decoupling of erosion and precipitation in the Himalayas, *Nature*, *426*, 652–655, doi:10.1038/nature02187.

Carena, S., J. Suppe, and H. Kao (2002), Active décollement of Taiwan illuminated by small earthquakes and its control of first order topography, *Geology*, *30*, 935–938, doi:10.1130/0091-7613(2002)030<0935:ADOTIB>2.0.CO;2.

Chapple, W. M. (1978), Mechanics of thin-skinned fold-and-thrust belts, *Geol. Soc. Am. Bull.*, *89*, 1189–1198, doi:10.1130/0016-7606(1978)89<1189:MOTFB>2.0.CO;2.

Cundall, P., and M. Board (1988), A microcomputer program for modeling of large-strain plasticity problems, in *Numerical Methods in Geomechanics: Proceedings of the 6th International Conference on Numerical Methods in Geomechanics*, vol. 2, edited by C. Swododa, pp. 101–108, Balkemapp, Innsbruck, Austria.

Dadson, S. J., et al. (2003), Links between erosion, runoff variability and seismicity in the Taiwan Orogen, *Nature*, *426*, 648–651, doi:10.1038/nature02150.

Dahlen, F. A. (1984), Noncohesive critical coulomb wedges: An exact solution, *J. Geophys. Res.*, *89*, 10,125–10,133, doi:10.1029/JB089iB12p10125.

Dahlen, F. A., and T. D. Barr (1989), Brittle frictional mountain building: 1. Deformation and mechanical energy budget, *J. Geophys. Res.*, *94*, 3906–3922, doi:10.1029/JB094iB04p03906.

Dahlen, F. A., and J. Suppe (1988), Mechanics, growth and erosion of mountain belts, in *Processes in Continental Lithospheric Deformation*, edited by S. P. Clark Jr. et al., *Spec. Pap. Geol. Soc. Am.*, *218*, 161–178.

Dahlen, F. A., J. Suppe, and D. Davis (1984), Mechanics of fold-and-thrust belts and accretionary wedges: Cohesive Coulomb wedge theory, *J. Geophys. Res.*, *89*, 10,087–10,101, doi:10.1029/JB089iB12p10087.

Davis, D. M., and R. J. Lillie (1994), Changing mechanical response during continental collision: Active examples from the foreland thrust belts of Pakistan, *J. Struct. Geol.*, *16*, 21–34, doi:10.1016/0191-8141(94)90015-9.

Davis, D., J. Suppe, and F. A. Dahlen (1983), Mechanics of fold-and-thrust belts and accretionary wedges, *J. Geophys. Res.*, *88*, 1153–1172, doi:10.1029/JB088iB02p01153.

Ege, H., E. R. Sobel, E. Scheuber, and V. Jacobshagen (2007), Exhumation history of the southern Altiplano plateau (southern Bolivia) constrained by apatite fission track thermochronology, *Tectonics*, *26*, TC1004, doi:10.1029/2005TC001869.

Fuller, C. W., S. D. Willett, D. Fisher, and C. Y. Lin (2006), A thermomechanical wedge model of Taiwan constrained by fission-tract thermochronometry, *Tectonophysics*, *425*, 1–24, doi:10.1016/j.tecto.2006.05.018.

Galewsky, J., C. P. Stark, S. Dadson, C.-C. Wu, A. H. Sobel, and M.-J. Horng (2006), Tropical cyclone triggering of sediment discharge in Taiwan, *J. Geophys. Res.*, *111*, F03014, doi:10.1029/2005JF000428.

Grujic, D., I. Coutand, B. Bookhagan, S. Bonnet, A. Blythe, and D. Duncan (2006), Climatic forcing of erosion, landscape, and tectonics in the Bhutan Himalayas, *Geology*, *34*, 801–804, doi:10.1130/G22648.1.

Hicks, D. D., J. Hill, and U. Shanker (1996), Variation of suspended sediment yields around New Zealand: The relative importance of rainfall and geology, *IHAS Publ.*, *236*, 149–156.

Hilley, G. E., and M. R. Strecker (2004), Steady state erosion of critical Coulomb wedges with applications to Taiwan and the Himalaya, *J. Geophys. Res.*, *109*, B01411, doi:10.1029/2002JB002284.

Hoth, S., J. Adam, N. Kukowski, and O. Oncken (2006), Influence of erosion on the kinematics of bivergent orogens: Results from scaled sandbox simulations, in *Tectonics, Climate and Landscape Evolution, Penrose Conference Series*, edited by S. Willett et al., *Spec. Pap. Geol. Soc. Am.*, *398*, 201–225, doi:10.1130/2006.2398(12).

Hoth, S., A. Hoffmann-Rothe, and N. Kukowski (2007), Frontal accretion: An internal clock for bivergent wedge deformation and surface uplift, *J. Geophys. Res.*, *112*, B06408, doi:10.1029/2006JB004357.

Hovius, N., C. P. Stark, and P. A. Allen (1997), Sediment flux from a mountain belt derived by landslide mapping, *Geology*, *25*, 231–234, doi:10.1130/0091-7613(1997)025<0231:SFFAMB>2.3.CO;2.

Hubert-Ferrari, A., J. Suppe, J. Van Der Woerd, X. Wang, and H. Lu (2005), Irregular earthquake cycle along the southern Tianshan front,

Aksu area, China, *J. Geophys. Res.*, *110*, B06402, doi:10.1029/2003JB002603.

Itasca (2006), FLAC^{3D} (Fast Lagrangian Analysis of Continua in 3 Dimensions, version 3.1), Minneapolis, Minn.

Koons, P. O. (1990), Two-sided orogen: Collision and erosion from the sandbox to the Southern Alps, New Zealand, *Geology*, *18*, 679–682, doi:10.1130/0091-7613(1990)018<0679:TSOCAE>2.3.CO;2.

Koons, P. O. (1995), Modeling the topographic evolution of collisional mountain belts, *Annu. Rev. Earth Planet. Sci.*, *23*, 375–408, doi:10.1146/annurev.ea.23.050195.002111.

Koons, P. O., P. K. Zeitler, C. P. Chamberlain, D. Craw, and A. S. Melzer (2002), Mechanical links between erosion and metamorphism in Nanga Parbat, Pakistan Himalaya, *Am. J. Sci.*, *302*, 749–773, doi:10.2475/ajs.302.9.749.

Koons, P. O., R. J. Norris, D. Craw, and A. F. Cooper (2003), Influence of exhumation on the structural evolution of transpressional plate boundaries: An example from the Southern Alps, New Zealand, *Geology*, *31*, 3–6, doi:10.1130/0091-7613(2003)031<0003:IOEOTS>2.0.CO;2.

Liu, T. K., S. Hsieh, Y.-G. Chen, and W. S. Chen (2001), Thermo-kinematic evolution of the Taiwan oblique-collision mountain belt as revealed by zircon fission track dating, *Earth Planet. Sci. Lett.*, *186*, 45–56, doi:10.1016/S0012-821X(01)00232-1.

Lock, J. (2007), Interpreting low-temperature thermochronometric data in fold-and-thrust belts: An example from the Western Foothills, Taiwan, Ph.D. thesis, 196 pp., Univ. of Wash., Seattle.

Marques, F. O., and P. R. Cobbold (2002), Topography as a major factor in the development of arcuate thrust belts: Insights from sandbox experiments, *Tectonophysics*, *348*, 247–268, doi:10.1016/S0040-1951(02)00077-X.

Masaferro, J. L., M. Bulnes, J. Poblet, and G. P. Eberli (2002), Episodic folding inferred from syntectonic carbonate sedimentation: The Santaren anticline, Bahamas foreland, *Sediment. Geol.*, *146*(1–2), 11–24, doi:10.1016/S0037-0738(01)00163-4.

Masek, J. G., B. L. Isacks, T. L. Gubbels, and E. J. Fielding (1994), Erosion and tectonics at the margins of continental plateaus, *J. Geophys. Res.*, *99*, 13,941–13,956, doi:10.1029/94JB00461.

Moresi, L., D. May, and V. Lemiale (2006), Extension from 2D to 3D, *Eos Trans. AGU*, *87*(52), Fall Meet. Suppl., Abstract T23F-01.

Mouthereau, F., O. Lacombe, B. Deffontaines, J. Angleier, H. T. Chu, and C. T. Lee (1999), Quaternary transfer faulting and belt front deformation at Pakuashan (western Taiwan), *Tectonics*, *18*, 215–230, doi:10.1029/1998TC900025.

Mouthereau, F., B. Deffontaines, O. Lacombe, and J. Angleier (2002), Variations along the strike of the Taiwan thrust belt: Basement control of structural style, wedge geometry and kinematics, in *Geology and Geophysics of an Arc-Continent collision, Taiwan, Republic of China*, edited by T. B. Byrne and S.-S. Lin, *Spec. Pap. Geol. Soc. Am.*, *358*, 35–58.

Mueller, K., Y.-G. Chen, and G. Kier (2001), Erosion-induced backstepping and reactivation of the Chelungpu thrust: Implications for patterns of modern strain release in west-central Taiwan, *Eos Trans. AGU*, *82*(47), Fall Meeting Supplements, Abstract T32A-0878.

Mueller, K., Y.-G. Chen, and L. Powell (2002), Modern strain and structural architecture of the central Taiwanese orogen-Evidence for active backstepping in response to erosion?, *Eos Trans. AGU*, *83*(47), Fall Meet. Suppl., Abstract T61B-1279.

Mueller, K., T. Wilcox, and Y.-G. Chen (2006), Subcritical thrust wedge development in west-central Taiwan in response to rapid erosion of synorogenic sediments, *Eos Trans. AGU*, *87*(52), Fall Meet. Suppl., Abstract T11A-0433.

Naylor, M., and H. D. Sinclair (2007), Punctuated thrust deformation in the context of doubly vergent thrust wedges: Implications for the localization of uplift and exhumation, *Geology*, *35*, 559–562, doi:10.1130/G23448A.1.

Powell, L., K. K. Mueller, and Y.-G. Chen (2003), Geomorphic constraints on patterns of shortening and erosion in the Puli Basin: Hinterland of the Central Taiwan Thrust Belt, *Eos Trans. AGU*, *83*(47), Fall Meet. Suppl., Abstract T61B-1270.

Safran, E. B., A. Blythe, and T. Dunne (2006), Spatially variable exhumation rates in orogenic belts: An Andean example, *J. Geol.*, *114*, 665–681, doi:10.1086/507613.

Sheaf, M. A., L. Serpa, and T. L. Pavlis (2003), Exhumation rates in the St. Elias Mountains, Alaska, *Tectonophysics*, *367*, 1–11, doi:10.1016/S0040-1951(03)00124-0.

Simoes, M., and J. P. Avouac (2006), Investigating the kinematics of mountain building in Taiwan from the spatiotemporal evolution of the foreland basin and western foothills, *J. Geophys. Res.*, *111*, B10401, doi:10.1029/2005JB004209.

Simoes, M., J. P. Avouac, and Y.-G. Chen (2007a), Slip rates on the Chelungpu and Chushiang thrust faults inferred from a deformed strath terrace along the Dungpuna river, west central Taiwan, *J. Geophys. Res.*, *112*, B03S10, doi:10.1029/2005JB004200.

Simoes, M., J. P. Avouac, Y.-G. Chen, A. K. Singhvi, C.-Y. Wang, M. Jaiswal, Y.-C. Chan, and S. Bernard (2007b), Kinematic analysis of the Pakuashan fault tip fold, west central Taiwan: Shortening rate and age of folding inception, *J. Geophys. Res.*, *112*, B03S14, doi:10.1029/2005JB004198.

Sinclair, H. D., M. Gibson, M. Naylor, and R. G. Morris (2005), Asymmetric growth of the Pyrenees revealed through measurement and modeling of orogenic fluxes, *Am. J. Sci.*, *305*, 369–406, doi:10.2475/ajs.305.5.369.

Soto, R., A. M. Casas-Sainz, and E. L. Pueyo (2006a), Along-strike variation of orogenic wedges associated with vertical axis rotations, *J. Geophys. Res.*, *111*, B10402, doi:10.1029/2005JB004201.

Soto, R., F. Storti, and A. M. Casas-Sainz (2006b), Impact of backstop thickness lateral variations on the tectonic architecture of orogens: Insights from sandbox analogue modeling and application to the Pyrenees, *Tectonics*, *25*, TC2005, doi:10.1029/2004TC001693.

Spotila, J. A., J. T. Buscher, A. J. Meigs, and P. W. Reiners (2004), Long-term glacial erosion of active mountain belts: Example of the Chugach-St. Elias Range, Alaska, *Geology*, *32*, 501–504, doi:10.1130/G20343.1.

Stockmal, G. S. (1983), Modeling of large scale accretionary wedge deformation, *J. Geophys. Res.*, *88*, 8271–8287, doi:10.1029/JB088iB10p08271.

Sung, Q., Y.-C. Chen, H. Tsai, Y.-G. Chen, and W.-S. Chen (2000), Comparison study on the coseismic deformation of the 1999 Chi-Chi earthquake and long-term stream gradient changes along the Chelungpu Fault in central Taiwan, *Terr. Atmos. Oceanic Sci.*, *11*, 735–750.

Suppe, J. (2007), Absolute fault and crustal strength from wedge tapers, *Geology*, *35*, 1127–1130, doi:10.1130/G24053A.1.

Thiede, R. C., B. Bookhagen, J. R. Arrowsmith, E. R. Sobel, and M. R. Strecker (2004), Climatic control on rapid exhumation along the southern Himalayan Front, *Earth Planet. Sci. Lett.*, *222*, 791–806, doi:10.1016/j.epsl.2004.03.015.

Thiede, R. C., J. R. Arrowsmith, B. Bookhagen, M. O. McWilliams, E. R. Sobel, and M. R. Strecker (2005), From tectonically to erosionally controlled development of the Himalayan orogen, *Geology*, *33*, 689–692, doi:10.1130/G21483.1.

Upton, P., and P. O. Koons (2007), Three-dimensional geodynamic framework for the central Southern Alps, New Zealand: Integrating geology, geophysics and mechanical observations, in *A Continental Plate Boundary: Tectonics at South Island, New Zealand*, *Geophys. Monogr. Ser.*, vol. 175, edited by D. Okaya, T. Stern, and F. Davey, pp. 255–272, AGU, Washington, D. C.

Upton, P., P. O. Koons, and D. Eberhart-Phillips (2003a), Extension and partitioning in an oblique subduction zone, New Zealand: Constraints from three-dimensional numerical modeling, *Tectonics*, *22*(6), 1068, doi:10.1029/2002TC001431.

Upton, P., K. J. Mueller, and P. O. Koons (2003b), Reorganization of strain in response to erosional forcing at intermediate scales: Puli Embayment, Western Taiwan, *Eos Trans. AGU*, *84*(46), Fall Meet. Suppl., Abstract T31F-0899.

Upton, P., P. O. Koons, D. Craw, M. Henderson, and R. L. Enlow (2009), Along-strike differences in the Southern Alps of New Zealand: Consequences of inherited variation in rheology, *Tectonics*, *28*, TC2007, doi:10.1029/2008TC002353.

Vermeer, P. A., and R. de Borst (1984), Non-associated plasticity for soils, concrete and rock, *Heron*, *29*, 1–64.

Whipple, K. X., and B. J. Meade (2004), Controls on the strength of coupling among climate, erosion, and deformation in two-sided, frictional orogenic wedges at steady state, *J. Geophys. Res.*, *109*, F01011, doi:10.1029/2003JF000019.

Wilcox, T., K. Mueller, and Y.-G. Chen (2007), Systematic variations in synorogenic fill architecture and fault offsets along strike across the Puli topographic embayment: Quaternary strain gradients in the central Western Foothills and Taiwanese foreland basin, *Eos Trans. AGU*, *88*(52), Fall Meet. Suppl., Abstract T32C-07.

Willett, S. D. (1999), Orogeny and orography: The effect of erosion on the structure of mountain belts, *J. Geophys. Res.*, *104*, 28,957–28,981, doi:10.1029/1999JB900248.

Willett, S. D., and C. Beaumont (1994), Subduction of Asian lithospheric mantle beneath Tibet inferred from models of continental collision, *Nature*, *369*, 642–645, doi:10.1038/369642a0.

Willett, S. D., C. Beaumont, and P. Fullsack (1993), Mechanical model for the tectonics of doubly vergent orogens, *Geology*, *21*, 371–374, doi:10.1130/0091-7613(1993)021<0371:MMFTTO>2.3.CO;2.

Willett, S. D., D. Fisher, C. Fuller, E.-C. Yeh, and C. Y. Lu (2003), Orogen kinematics and erosion rates in Taiwan from thermochronometric data, *Geology*, *31*, 945–948, doi:10.1130/G19702.1.

Wobus, C. W., K. V. Hodges, and K. X. Whipple (2003), Has focused denudation sustained active thrusting at the Himalayan topographic front?, *Geology*, *31*, 861–864, doi:10.1130/G19730.1.

Wobus, C. W., A. Heimsath, K. X. Whipple, and K. V. Hodges (2005), Active out-of-sequence thrust faulting in the central Nepalese Himalaya, *Nature*, *434*, 1008–1011, doi:10.1038/nature03499.

Wu, C.-C., and Y.-H. Kuo (1999), Typhoons affecting Taiwan: Current understanding and future challenges, *Bull. Am. Meteorol. Soc.*, *80*, 67–80, doi:10.1175/1520-0477(1999)080<0067:TATCUA>2.0.CO;2.

Yang, K.-M., S.-T. Huang, J.-C. Wu, H.-H. Ting, W.-W. Mei, M. Lee, H.-H. Hsu, and C.-J. Lee (2007), 3D geometry of the Chelungpu thrust system in central Taiwan: Its implications for active tectonics, *Terr. Atmos. Oceanic Sci.*, *18*, 143–181, doi:10.3319/TAO.2007.18.2.143(TCDP).

Yanites, B. J., G. E. Tucker, K. Mueller, T. Wilcox, and Y.-G. Chen (2007), Structural controls on channel geometry and dynamics in the Peikang River, central Taiwan, *Eos Trans. AGU*, *88*(52), Fall Meet. Suppl., Abstract H41D-0762.

Yeh, Y. H., and H. Y. Yen (1992), *Bouguer anomaly map of Taiwan*, Inst. Earth. Sci., Acad. Sin, Taipei, Taiwan.

Yue, L.-F., J. Suppe, and J.-H. Hung (2005), Structural geology of a classic thrust belt earthquake: The 1999 Chi-Chi earthquake Taiwan (M_w = 7.6), *J. Struct. Geol.*, *27*, 2058–2083, doi:10.1016/j.jsg.2005.05.020.

Yue, L.-F., J. Suppe, and J.-H. Hung (2009), Two contrasting kinematic styles of active folding above thrust ramps, western Taiwan, in *Thrust-Related Folding*, edited by K. McClay, J. H. Shaw, and J. Suppe, *APPG Memoir*, in press.

Zeitler, P. K., et al. (2001), Crustal reworking at Nanga Parbat, Pakistan; metamorphic consequences of thermal-mechanical coupling facilitated by erosion, *Tectonics*, *20*, 712–728, doi:10.1029/2000TC001243.

Y.-G. Chen, Department of Geosciences, Taiwan National University, Taipei, Taiwan.

K. Mueller, Department of Geological Sciences, University of Colorado, Boulder, CO 80309-0399, USA.

P. Upton, GNS Science, Private Bag 1930, Dunedin, 9054, New Zealand. (p.upton@gns.cri.nz)